Tellus (1994), 46B, 103–122
Printed in Belgium – all rights reserved

TELLUS
ISSN 0280–6509

Carbon uptake experiments with a zonally-averaged global ocean circulation model

By THOMAS F. STOCKER*, and WALLACE S. BROECKER, *Lamont-Doherty Earth Observatory of Columbia University, Palisades, New York, USA*, and DANIEL G. WRIGHT, *Bedford Institute of Oceanography, Dartmouth, Nova Scotia, Canada*

(Manuscript received 25 March 1993; in final form 4 October 1993)

ABSTRACT

A model which simulates the zonally averaged thermohaline circulation in the major ocean basins and includes the balance of stable and decaying tracers, is presented. The model is used to estimate oceanic uptake of tracers due to transiently varying atmospheric concentrations, with steady thermohaline circulation. $2 \times CO_2$-experiments with an inorganic carbon cycle component yield an evolution that is consistent with results from 3-dimensional models on time scales of decades to millennia. The model's average uptake from 1980–1989 is 2.1 Gt C yr^{-1} when the industrial evolution of pCO_2 in the atmosphere is prescribed. Only about 10% of excess carbon is taken up by waters sinking in the North Atlantic but 30% by waters sinking in the Southern Ocean. The influence of vertical and horizontal mixing processes on the uptake in various regions the ocean is investigated. Uptake experiments of bomb-produced radiocarbon demonstrate possible limitations of the model. Agreement with the observations can be obtained if a parameterization is introduced that accounts for the near-surface meridional mixing of tracers due to the wind-driven circulation. Inventories and penetration depth of bomb radiocarbon are compared with estimates from 3-dimensional model simulations and observations. Global uptake is close to these estimates, however, inventories in the Southern Ocean are considerably larger.

1. Introduction

The thermohaline circulation of the world ocean is the most important pathway by which tracers are exchanged between the surface and the large reservoir of the deep ocean: major uptake occurs in regions where deep water is formed. Also, much of the poleward oceanic heat transport is caused by the thermohaline circulation and thus represents an important component of the climate system. During the last few years evidence has been accumulated from the analysis of paleoclimatic data (Broecker and Denton, 1989) and various ocean model experiments (Bryan, 1986; Maier-Reimer and Mikolajewicz, 1989; Stocker et al., 1992a) that the variability of the thermohaline circulation is probably responsible for large-scale and abrupt climatic change. Therefore, the question arises to what extent changes in deep water formation could influence the distribution of tracers in the ocean and how atmospheric concentrations would evolve. In the case of carbon dioxide which enhances the greenhouse effect, a suite of feedback mechanisms could be triggered (Manabe and Stouffer, 1993).

Before these important questions can be addressed, however, it is necessary that efficient ocean circulation models be available with which the distribution of various tracers can be simulated. These models must then be tested for two different characteristics. First, are the modelled steady state distributions of tracers consistent with those observed? Second, are uptake rates of tracers with transient atmospheric concentrations consistent with observations?

* Corresponding author, now at: Physics Institute, University of Bern, 3012 Bern, Switzerland.

The purpose of this paper is to present such a model including geochemical tracers and to assess its performance with respect to tracer uptake. Here we distinguish between time scales associated with changes of the thermohaline overturning (such as natural variability or mode changes) and time scales related to changing atmospheric concentration of tracers (such as carbon dioxide, radiocarbon of chloro-fluoro-carbons). This study is restricted to transient changes of tracer concentrations with the thermohaline circulation held constant. This should establish the basis for later investigations on the effects of changes of the thermohaline circulation on the global distribution of tracers in the ocean and atmosphere. We will describe the model components and present two applications where uptake rates of excess atmospheric tracers, carbon dioxide and bomb radiocarbon, are studied for different circulation patterns.

The model may be integrated for many thousands of years and combines simplified ocean dynamics with geochemical processes. Such physical-geochemical models are valuable tools to investigate systematically the interaction between different components of the climate system. Further, equilibrium states of a physical-geochemical climate model are much more tightly constrained than those of ocean-atmosphere models by a more extensive dataset defining a given climate. For example, radiocarbon is an additional check on the quality of the steady-state deep circulation simulated in an ocean model under present-day surface forcing, an approach that has been employed before (Maier-Reimer and Hasselmann, 1987; Toggweiler et al., 1989; Stocker et al., 1992b).

Early studies that include deep ocean circulation in combination with geochemical components are the box models of Oeschger et al. (1975), Bolin et al. (1983) and Siegenthaler (1983). The ocean circulation is accounted for by prescribing mass fluxes between the model boxes. The efficiency of these box models allows integration over long times; however, fully transient experiments may not be reliable because the circulation state of the ocean must be prescribed. During the last few years, several groups have implemented geochemical components into 3-dimensional ocean general circulation models (OGCMs). Maier-Reimer and Hasselmann (1987) coupled an inorganic carbon cycle model to their large-scale global general circulation model. Uptake of carbon dioxide was simulated and related to observations of the atmospheric pCO_2 increase. Their results are in broad agreement with estimates from simpler box-diffusion models (Oeschger et al., 1975, Siegenthaler, 1983). An alternative approach reaching quantitatively similar conclusions was presented by Sarmiento et al. (1992). They simulate CO_2 uptake with an inorganic perturbation model coupled to the Princeton global OGCM.

More recently, a generic nutrient, total carbon, alkalinity and oxygen were taken as the minimum building blocks of an organic carbon cycle model (Bacastow and Maier-Reimer, 1990), and the resulting steady-state distributions of the modeled tracers were shown to be in fair agreement with observations. Subsequent improvements especially with respect to an increased ventilation of the North Atlantic have resulted in more realistic tracer fields as (Heinze et al., 1991). They also estimate the dependence of atmospheric pCO_2 on the ocean circulation and on parameters determining exchange, mixing and cycling of nutrients. While these 3-dimensional physical-geochemical models represent the most complete approach to the problem, integrations over many thousands of years are computationally very expensive, and important sensitivity studies for transient evolution are virtually impossible. Thus, models are called for that are intermediate between box models and 3-dimensional models.

Recently, progress has been made by developing zonally averaged, dynamical ocean models for the global thermohaline circulation (Marotzke et al., 1988; Wright and Stocker, 1991, 1992 (WS92 henceforth); Stocker et al., 1992a, b). The strength of these models is their efficiency combined with a solution structure that is similar to 3-dimensional global OGCMs. Also, oceanic variability on at least the century time scale and longer can be studied with these models (Mysak et al., 1993). Limitations do exist and care must be taken not to over-interpret results from lower-order numerical models, but such models are the most suitable tools presently available to undertake extensive quantitative studies of climatic evolution involving the ocean's thermohaline circulation.

The plan of this paper is as follows. In Section 2, the ocean and tracer components of the model are discussed. An inorganic carbon cycle is coupled

to the climate model in Section 3, and results of carbon dioxide uptake experiments are shown to be consistent with previous studies. Bomb radiocarbon uptake experiments are discussed in Section 4, and conclusions follow in Section 5.

2. Model description

Global models of the thermohaline circulation must resolve at least Pacific and Atlantic individually in order to simulate the fundamentally different conditions in these two basins. In this model the world ocean is represented by three different ocean basins which are connected via a Southern Ocean south of 40°S (Fig. 1). A meridional ridge is included in the Southern Ocean at depths greater than 2500 m, and a resolution of 14 boxes meridionally and 14 layers vertically is selected. Because we are concerned with the uptake and release of tracers, we modified ocean depth and surface area in the simplest possible way to approach the estimates of Menard and Smith (1966) to within 5%. Ocean depth is reduced to 4000 m and the angular extent of Pacific, Atlantic and Indian Ocean are 140°, 70° and 75°, respectively. These new values do not affect any of the conclusions drawn in earlier papers using this model. They do, however, change model values slightly, e.g., the maximum meridional overturning obtained under a given surface forcing.

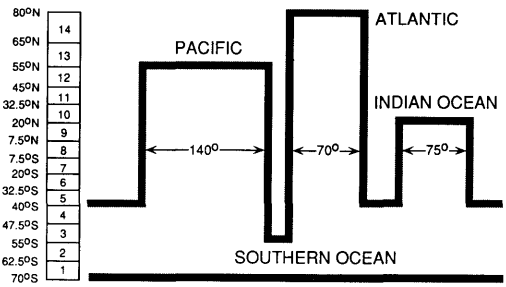

Fig. 1. Geometry and meridional resolution of the ocean model. The ocean basin has area and volume that are within 5% of the observed estimates. The vertical resolution is given in Table 1.

The present model is based on the zonally averaged ocean model presented by WS92. The ocean component consists of the zonally averaged balance equations of horizontal momentum, mass, temperature and salt for each ocean basin (Fig. 1); the hydrostatic relation and Boussinesq assumptions are invoked. The momentum balance is diagnostic, and time dependence enters through the advection-diffusion equations for temperature and salt. The density field, calculated using a nonlinear, pressure-dependent equation of state, and the surface wind stress determine the total

Table 1. *Ocean model parameters; identical diffusivities are used for potential temperature, salinity, total carbon and radiocarbon*

Ocean model parameters		
ρ_*	reference density	1027.8 kg m^{-3}
a	Earth's radius	6371 km
K_V	vertical diffusivity	0.4×10^{-4} m^2 s^{-1}
ε_0	closure parameter	0.45
H	ocean depth	4000 m
Δz	mixed layer depth	50 m
	bottom of model cells [m]	50, 100, 150, 250, 500, 750, 1000, 1250, 1500, 2000, 2500, 3000, 3500, 4000
	ridge in Southern Ocean	2500 m depth from 70°S–55°S
	relaxation time for T and S	50 days
C^*	restoring surface value for ^{14}C	$1000‰$
τ	relaxation time for ^{14}C	5 or 6 years
λ	decay constant for ^{14}C	3.84×10^{-12} s^{-1}
k	gas exchange rate for ΣC	0.067 mole m^{-2} yr^{-1} ppm^{-1}

The closure parameter ε_0 relates the east-west pressure difference to the meridional density gradient (see Wright and Stocker (1992) for details).

meridional overturning circulation. The ocean model parameters used in this paper are given in Table 1.

Upon zonally averaging the zonal momentum equation, the east-west pressure difference appears and must be estimated using a closure scheme. Wright and Stocker (1991) argued, based on the analysis of the steady-state density field of a 3-dimensional OGCM, that the east-west pressure difference can be linearly related to the meridional pressure gradient in the absence of wind stress, and WS92 use an analogous relation for density when wind stress is included. A number of subsequent studies have demonstrated that this is a reasonable parameterization. This qualification is based on the comparison of present-day steady states with observations, and on the similarity of the solution structure and the transient behavior between the zonally averaged and the 3-dimensional ocean circulation models (see WS92 for references).

The model contains a number of different mixing processes. Explicit vertical and horizontal diffusion is included, and numerical diffusion is corrected for using a mass-conserving flux correction scheme (see WS92). Zonal wind stress induces surface-enhanced meridional circulations which provide additional vertical mixing particularly in the top 400 m. Bomb radiocarbon experiments (Section 4) highlight the fact that meridional mixing due to wind-driven gyres must also be parameterized in this zonally averaged model in order to obtain surface concentrations that are consistent with the observations.

Let us estimate the magnitude of horizontal diffusivity that accounts for meridional mixing due to wind-driven gyres. Assuming a circulation of 40 Sv in a latitude band between 20° and 40° latitude extending over 60° angular width and 500 m depth yields a recirculation time of about 5 years. If the meridional mixing takes place over a distance of 20° latitude, a near surface horizontal diffusivity of order $3 \times 10^4\ m^2\ s^{-1}$ is obtained. We assume a depth-dependent horizontal diffusivity of the form

$$K_H(z) = \frac{K_s + K_d}{2} - \frac{K_s - K_d}{\pi} \arctan\left(\frac{z - z_0}{d}\right), \quad (1)$$

where $K_s = 3 \times 10^4\ m^2 s^{-1}$ and $K_d = 10^3\ m^2\ s^{-1}$ are surface and deep horizontal diffusivities, $z_0 =$ 300 m and $d = 50$ m are a penetration depth and scale thickness of the diffusivity structure accounting for gyral mixing. This formulation is applied north of 40°S; south of 40°S we set $K_H = K_d$.

Restoring boundary conditions (with identical time scales for temperature and salinity) are widely used to find a unique steady-state of the ocean circulation whose surface values of temperature and salinity are close to the observed. Heat and freshwater fluxes are taken to be proportional to the local deviation of the modelled surface values from observations. Here, these conditions are determined by the annual-mean, zonally averaged temperatures and salinities at 30 m given by Levitus (1982) with a restoring time scale of 50 days.

The ocean model is integrated for 4000 years to obtain a steady state under restoring surface boundary conditions. The meridional overturning streamfunction at steady state exhibits the typical "conveyor belt" circulation which results under present-day forcing (Fig. 2). Its strength and details of its structure depend on the north-south buoyancy contrast, which may be influenced by specification of the high-latitude surface salinities and the parameterization of surface mixing processes. In an earlier study (Stocker et al., 1992b) we found that with the zonal and annual mean surface salinity values given by Levitus, the deep water is formed only in the North Atlantic. Deep water mass distributions are more realistic if surface salinities in the areas of deep water formation (south of 62.5°S and north of 65°N) are adjusted to the observed values of newly formed deep water.

Five steady-state circulations (A, B, D–F, see Table 2) are considered. State A (Fig. 2a) is the "best tuned" circulation: the latitude-depth

Table 2. *Summary of the characteristics of the different steady states of the thermohaline circulation*

State	A	B	C	D	E	F
Figure	2a	2b	—	2c	2d	2e
wind	yes	yes	yes	no	no	yes
K_s [$m^2\ s^{-1}$]	3×10^4	1×10^3	1×10^3	1×10^3	1×10^3	1×10^3
K_d [$m^2\ s^{-1}$]	1×10^3	1×10^3	1×10^3	1×10^3	1×10^3	1×10^3
S_1^* [psu]	34.6	34.6	34.6	34.6	34.9	34.9
S_2^* [psu]	34.9	34.9	34.9	34.9	34.5	34.5
τ [yr]	6	6	5	5	5	5

K_s and K_d denote surface and deep horizontal diffusivities, S_1^* and S_2^* are the restoring salinities at 65°S and 72°N, respectively, and τ is the relaxation time for ^{14}C.

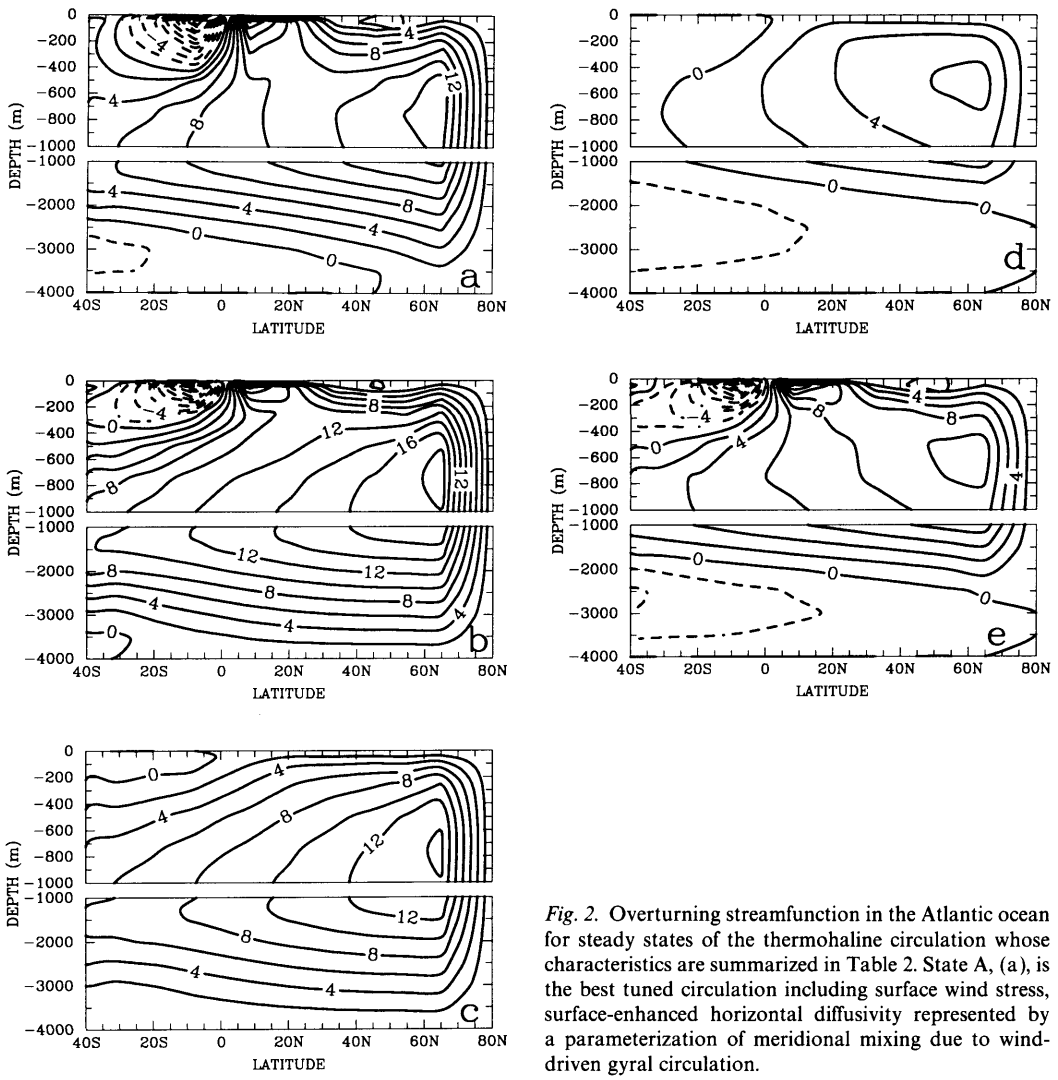

Fig. 2. Overturning streamfunction in the Atlantic ocean for steady states of the thermohaline circulation whose characteristics are summarized in Table 2. State A, (a), is the best tuned circulation including surface wind stress, surface-enhanced horizontal diffusivity represented by a parameterization of meridional mixing due to wind-driven gyral circulation.

distributions of temperature, salinity and radiocarbon are consistent with observations in the modern ocean. Deep water is formed in both high latitudes, water is sinking at a rate of about 14 Sv ($1\ \mathrm{Sv} = 10^6\ \mathrm{m}^3\ \mathrm{s}^{-1}$) in the North Atlantic from where it flows into the other basins. About 2 Sv of Antarctic Bottom Water (AABW) enter the Atlantic Ocean. The model reproduces quite well the global structure of the thermohaline circulation. State B (Fig. 2b) exhibits increased meridional gradients of surface temperature and salinity and a stronger conveyor belt because horizontal diffusivity at the surface is reduced. The circulation of state C is identical to B. Wind forcing is then switched off in state D (Fig. 2c) and overturning is weakened. In state E (Fig. 2d), the north-south buoyancy contrast has been modified by adjusting the high-latitude restoring salinities: overturning in the Atlantic is shallow and decreases to about 6 Sv, and AABW fills the deep ocean. For state F (Fig. 2e) winds are turned on again and overturning is almost doubled but the influence on the composition of the deep water is minor.

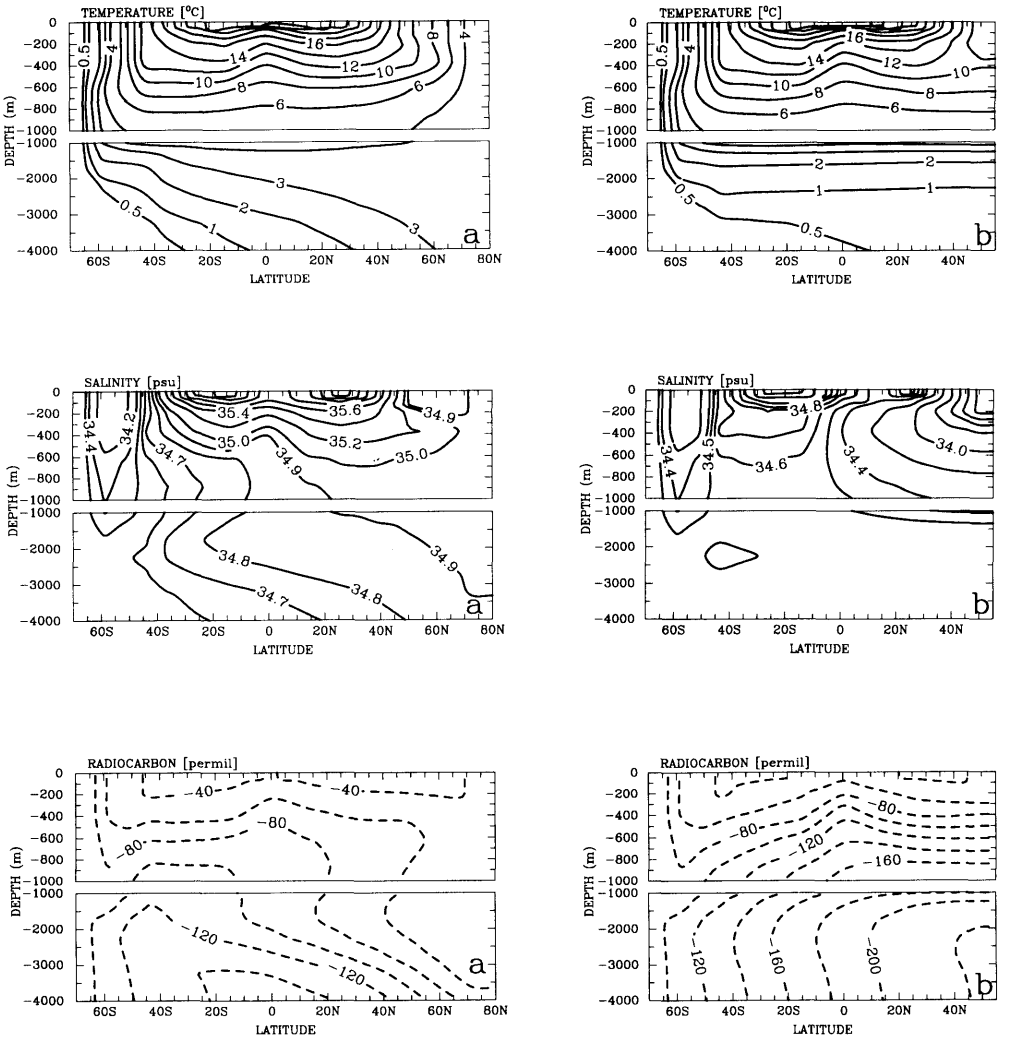

Fig. 3. The latitude-depth sections of potential temperature, salinity and radiocarbon in the Atlantic, (a), and the Pacific, (b), for circulation state A.

We include the balance of an arbitrary tracer C, which satisfies

$$\frac{\partial C}{\partial t}+\frac{1}{a\Lambda\cos\phi}\frac{\partial(\cos\phi v\Lambda C)}{\partial\phi}+\frac{\partial wC}{\partial z}$$
$$=\frac{1}{a^2\Lambda\cos\phi}\frac{\partial}{\partial\phi}\left(\cos\phi\Lambda K_{\mathrm{H}}\frac{\partial C}{\partial\phi}\right)$$
$$+\frac{\partial}{\partial z}K_{\mathrm{V}}\frac{\partial C}{\partial z}-\lambda C+q^{\mathrm{conv}}, \qquad (2)$$

where all quantities are zonal averages, (ϕ, z) are latitude-depth coordinates with z positive upwards, Λ is the angular width of the basin, a is the radius of the Earth, (v, w) are the meridional and vertical velocities, and K_{H} and K_{V} are horizontal and vertical diffusivities. In this study, we consider total carbon and radiocarbon as tracers. The parameter λ is a decay constant and is set to $\lambda = \ln 2/5730$ yr for ^{14}C, and $\lambda = 0$ for total

carbon. Vertical fluxes due to convection are denoted by q^{conv}.

No-flux conditions for a tracer are applied at the bottom and lateral boundaries of the basin, while at the surface a restoring boundary condition of the form

$$F = \frac{H_M}{\tau}(C - C^*), \tag{3}$$

is applied. F is the vertical tracer flux (positive upward), H_M is the prescribed depth of a well-mixed surface layer, τ is a restoring time and C^* is a restoring value which is linked to the atmospheric concentration and may vary in time and space (see Section 4). The values of the parameters in (3) depend on the tracer considered. For each of the steady state circulations in Fig. 2 the model is integrated for another 10,000 years to allow total carbon and radiocarbon to equilibrate.

Fig. 3 displays the latitude-depth distributions of temperature, salinity and radiocarbon for steady state A. In the Atlantic (Fig. 3a) the temperature structure is in close agreement with the zonal means given by Levitus (1982): the 4°C isotherm reaches about 1200 m, and the 18°C isotherm is not deeper than 200 m. The salinity structure exhibits the three principal water masses in the Atlantic with fresher AABW below saltier NADW and again fresher Antarctic Intermediate Water. The distribution of radiocarbon (in $\Delta^{14}C$ units, see Section 4) is in fair agreement with the latitude-depth section obtained from GEOSECS. However, waters below 3000 m in the low latitudes are too old.

The same fields are also given for the Pacific (Fig. 3b). Deep ocean temperatures are now colder than in the Atlantic. The presence of a region with small salinity gradients in the low latitudes at about 1000 m is consistent with the zonally averaged data of Levitus (1982). Radiocarbon is also in broad agreement with the GEOSECS data in that waters at depth become progressively older towards the North Pacific. The deep-ocean gradients, however, indicate that younger waters from the deep Southern Ocean flow northward too slowly. In spite of the many simplification of this circulation model, satisfactory agreement with observations is found for the "best tuned" state.

3. Inorganic carbon cycle

3.1. Model description

We incorporate into the ocean model the inorganic carbon cycle model described by Maier-Reimer and Hasselmann (1987). Chemical equilibria are considered only in the surface layer of the ocean where the oceanic pCO_2 is determined from the carbonate system. The chemical equilibria are given by

$$H_2O + CO_2 \rightleftarrows H^+ + HCO_3^-, \tag{4a}$$

$$HCO_3^- \rightleftarrows H^+ + CO_3^=, \tag{4b}$$

$$H_2O \rightleftarrows H^+ + OH^-, \tag{4c}$$

$$H_2OB(OH)_3 \rightleftarrows H^+ + B(OH)_4^-, \tag{4d}$$

with dissociation constants defined as

$$K_1 = \frac{[H^+][HCO_3^-]}{[CO_2]}, \tag{5a}$$

$$K_2 = \frac{[H^+][CO_3^=]}{[HCO_3^-]}, \tag{5b}$$

$$K_W = [H^+][OH^-], \tag{5c}$$

$$K_B = \frac{[H^+][B(OH)_4^-]}{[H_2OB(OH)_3]}. \tag{5d}$$

These dissociation constants are strong functions of temperature, salinity and pressure (Mehrbach et al., 1973; Weiss, 1974). The system can be reduced assuming a total borate concentration of 4.106×10^{-4} mole kg^{-1} (at $S = 35$ psu; Culkin, 1965) and by defining two new variables, total carbon, ΣC, and alkalinity, A, according to

$$\Sigma C = [CO_2] + [HCO_3^-] + [CO_3^=], \tag{6a}$$

$$A = 2[CO_3^=] + [HCO_3^-] + [OH^-] + [B(OH)_4^-] - [H^+], \tag{6b}$$

(see Broecker and Peng, 1982). In an inorganic model, alkalinity is only affected by evaporation and precipitation at the ocean surface. Since the salinity field is subject to the same surface boundary condition, alkalinity can be recovered by simple scaling from salinity. We use mean values of $A = 2373$ μeq kg^{-1} and $S = 35$ psu (Takahashi et al., 1981). For steady state circulations (as is the

case throughout this paper) the surface freshwater flux integrated over the ocean basin vanishes, and hence no net exchange of salinity or alkalinity occurs.

For total carbon, eq. (2) is solved subject to the surface boundary condition

$$F_\Sigma = k(\mathrm{pCO}_2^{\mathrm{oce}} - \mathrm{pCO}_2^{\mathrm{atm}}), \tag{7}$$

where $k = 0.067$ mole m^{-2} yr^{-1} ppm^{-1} is a constant gas exchange rate (Broecker et al., 1985) and $\mathrm{pCO}_2^{\mathrm{oce}}$ and $\mathrm{pCO}_2^{\mathrm{atm}}$ are the partial pressures of carbon dioxide in the surface layer of the ocean and in the atmosphere, respectively. During spin-up, $\mathrm{pCO}_2^{\mathrm{atm}}$ is held fixed at the pre-industrial value of 280 ppm in order to find a consistent steady state carbon inventory of the ocean. In the mixed layer $\mathrm{pCO}_2^{\mathrm{oce}}$ is determined by solving the carbonate chemistry eqs. (5) and (6) as explained in Takahashi et al. (1980). Note that at steady state neither the model estimates of total carbon nor the absolute exchange fluxes can be directly compared to observations because a representation of the biological pump is not included in this formulation. This causes the surface-to-bottom contrast of total carbon to be only about 150 μmole kg^{-1} instead of about 400 μmole kg^{-1} as observed. While the model is effectively tuned to give a flux into the surface layer that is consistent with the pre-industrial atmospheric pCO_2, the vertical distribution of total carbon is incorrect. This and the absence of a biological pump prevents us from studying changes in the carbon inventory caused by transient changes of the thermohaline circulation with this model version.

To follow transient evolution of carbon dioxide in the atmosphere during a $2 \times \mathrm{CO}_2$-experiment we assume the balance

$$\frac{\partial}{\partial t}\mathrm{pCO}_2^{\mathrm{atm}} = \frac{F^{\mathrm{OA}}}{\rho_{\mathrm{A}} H_{\mathrm{A}}}, \tag{8}$$

where F^{OA} is given by

$$F^{\mathrm{OA}} = \frac{M_{\mathrm{A}}}{4\pi a^2}\int_{\mathrm{ocean}} F_\Sigma \, \mathrm{d}A, \tag{9}$$

$M_{\mathrm{A}} = 28.964$ kg kmole^{-1} denotes the molecular weight of air, and $H_{\mathrm{A}} = 8320$ m is a scale height of the atmosphere. Note that latitudinal dependence in the atmosphere is neglected and no biospheric reservoirs are included.

3.2. *Double-CO_2 experiments*

The following experiments serve to check model consistency with observations and previous studies on various time scales. Since uptake of carbon is difficult to compare directly with observations due to large uncertainties, we also compare the present model to other, more detailed 3-dimensional studies. Agreement of the basic carbon inventory with observations and 3-dimensional model results is demonstrated in Table 3. Important for later transient studies, however, is the evolution of the airborne fraction for a standard uptake experiment. The airborne fraction is defined as the ratio of the amount of perturbation carbon in the atmosphere to the amount of total perturbation carbon in the atmosphere-ocean system. As an example, we consider adjustments after $\mathrm{pCO}_2^{\mathrm{atm}}$ is instantly doubled which is equivalent to a pulse input of carbon into the atmosphere. The time scales involved in such an experiment range from

Table 3. *Comparison of some model characteristics with the Hamburg model (Maier-Reimer and Hasselmann, 1987), the Princeton model (Sarmiento et al., 1992) and estimates from observations (Sundquist, 1985; Siegenthaler and Oeschger, 1987)*

	State A	Hamburg	Princeton	Estimates
ΣC (ocean) [GtC]	37980	?	[perturbation model]	36600–38400
ΣC (atm.) [GtC]	603	615	?	594
pCO_2 [ppm]	280	290	280	280
r_∞	0.158	0.142	0.174	—

Inventories are given separately for the ocean and the atmosphere. r_∞ is the asymptotic airborne fraction.

order a year (related to surface processes) to millennia (related to the global overturning) and hence provide a good overall assessment of the model.

The evolution of the time-dependent airborne fraction, r, is displayed in Fig. 4 for circulation states A, D and E and compared to the results of the Hamburg (Maier-Reimer and Hasselmann, 1987) and Princeton models (Sarmiento et al., 1992). For state A, the initial uptake is faster than in the OGCMs (Fig. 4a), but already after 30 years, r is bracketed by that of the OGCMs resulting in an intermediate asymptotic airborne fraction of $r_\infty = 0.158$ (Fig. 4b, Table 3). Evolution of state B cannot be distinguished from A in this figure indicating that enhanced surface mixing is of minor importance for the uptake of total carbon (see also Table 5). Initial uptake is significantly slower for circulation D in which wind stress is switched off and surface horizontal mixing is not enhanced. However, beyond about 500 years differences between A and D become small as now the overturing (similar in both states) determines the evolution of the airborne fraction.

Since the Atlantic overturning rate of various OGCMs differs and since it is also sensitive to the surface buoyancy forcing which is not very well defined in high latitudes, it is worthwhile checking the influence of a much weaker conveyor belt on the uptake of CO_2. A $2 \times CO_2$-experiment for state E shows that the differences from state A in evolution of excess carbon uptake persist for a much longer time than in state D (Fig. 4b).

Meridional overturning thus influences in a significant way the rates of tracer uptake on time scales of decades to centuries. We have also tested the influence of vertical diffusivity on the uptake of CO_2 directly by increasing K_V from 0.4×10^{-4} $m^2 s^{-1}$ to $1 \times 10^{-4} m^2 s^{-1}$ and decreasing the closure parameter ε_0 from 0.45 to 0.15 (WS92) to obtain a similar circulation with a much deeper thermocline. The airborne fraction approaches r_∞ to within 1 % already after 1050 yr instead of over 1600 yr (state A) and is significantly faster than the Hamburg model.

3.3. *Industrial CO_2 uptake 1794–1990 AD*

Assuming that the circulation of the world ocean has not changed substantially over the last 250 years or so, we use the present inorganic model to simulate oceanic uptake of carbon dioxide during the industrial era. The atmospheric carbon dioxide concentration is prescribed by the spline fit of Siegenthaler and Oeschger (1987) as updated by Joos (personal communication), and integration starts from steady state in 1794 AD at 280.0 ppm with circulation state A (Fig. 2a). Note that all states in 1794 AD exhibit a net northward oceanic flux of total carbon across the equator. Absolute carbon fluxes are not expected to be simulated well in this inorganic carbon cycle model due to the absence of the biological pump which results

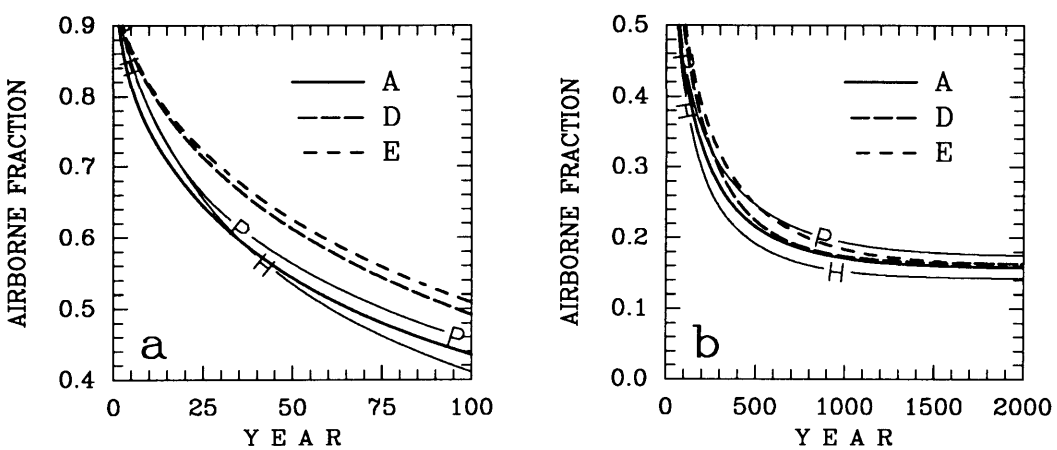

Fig. 4. Evolution of the airborne fraction of a $2 \times CO_2$-experiment for the first 100 year, (a), and 2000 years, (b), of integration using circulation state A, D and E. The results of the Hamburg (Maier-Reimer and Hasselmann, 1987) and Princeton GCMs (Sarmiento et al., 1992) are given for comparison.

Tellus B/46/2-3

Table 4. *Uptake rates and oceanic inventory changes in various models*

Mean uptake	State A	Princeton	H1	H2	B–D	Tans et al.
1980 [GtC/yr]	1.91	1.67	1.93	2.16	2.25	—
1980–1987 [GtC/yr]	2.08	—	—	—	—	$\leqslant 1.0$
total 1770–1980 [GtC]	100	92	107	123	123	—

Values are from Siegenthaler and Joos (1992). The models are the present zonally averaged model (state A), the Princeton 3-dimensional OGCM of Sarmiento et al. (1992), the box-diffusion models H1 (HILDA, variable vertical diffusivity) and H2 (HILDA, bomb calibrated) of Siegenthaler and Joos (1992), the box-diffusion (B–D) model of Siegenthaler and Oeschger (1987). An estimate using available observed pCO_2 differences is given by Tans et al. (1990). Note that in this model integration starts in 1794 whereas in the others it starts in 1770. Differences due to this are estimated to be less than 0.1 Gt.

in a significant underestimation of the vertical gradients of ΣC. Consequently, these results do not contradict Broecker and Peng (1992) who postulate a net southward flux of total carbon before the anthropogenic perturbation.

A comparison with other numerical models for anthropogenic uptake is shown in Table 4. Results of the present model are intermediate between the 3-dimensional study of Sarmiento et al. (1992), which exhibits a somewhat more sluggish uptake, and various versions of box-diffusion models. The uptake rates are clearly higher than those postulated by Tans et al. (1990). Table 5 gives the uptake and perturbation fluxes in 1990 broken up into various latitude bands. Time series of these diagnostic quantities for state A are presented in Fig. 5. Experiments were done for all circulation states of Fig. 2. The global uptake is dominated by the region between 45°S and 45°N where about 50% of the excess carbon is stored. Approximately the same fraction is also taken up by waters warmer than 5°C (Fig. 5c). As a consequence,

Table 5. *Industrial uptake experiment for the steady state circulations A, B, D–F of Fig. 2*

	1794					1990				
	A	B	D	E	F	A	B	D	E	F
Total uptake [GtC]	0	0	0	0	0	121	123	94	91	123
	total flux [Gt C yr^{-1}]					perturbation flux [Gt C yr^{-1}]				
global	0	0	0	0	0	−2.38	−2.42	−1.84	−1.77	−2.42
south of 45°S	−0.71	−0.42	−0.44	−0.55	−0.52	−0.81	−0.73	−0.62	−0.62	−0.73
north of 45°N (Atlantic)	−0.32	−0.28	−0.21	−0.11	−0.18	−0.16	−0.12	−0.16	−0.09	−0.09
north of 45°N (Pacific)	−0.12	−0.01	0.00	0.02	−0.01	−0.04	−0.02	−0.01	−0.03	−0.02
0–45°N	1.14	0.72	0.50	0.52	0.75	−0.62	−0.76	−0.48	−0.48	−0.76
45°S–0	0.01	−0.02	0.15	0.13	−0.04	−0.76	−0.78	−0.57	−0.56	−0.82
						% of excess carbon				
south of 45°S						32.9	32.5	37.8	40.6	34.4
north of 45°N (Atlantic)						9.9	10.4	11.6	7.6	7.6
north of 45°N (Pacific)						2.0	2.2	1.8	1.9	2.2
0–45°N						22.1	21.7	20.0	19.5	21.1
45°S–0						33.1	33.2	28.8	30.5	34.6
−2°C–5°C						43.0	44.1	53.0	50.6	41.7

The atmospheric pCO_2 is prescribed using the spline interpolation of Siegenthaler and Oeschger (1987); integration starts in 1794 AD. The uptake is broken up regionally as in Fig. 5.

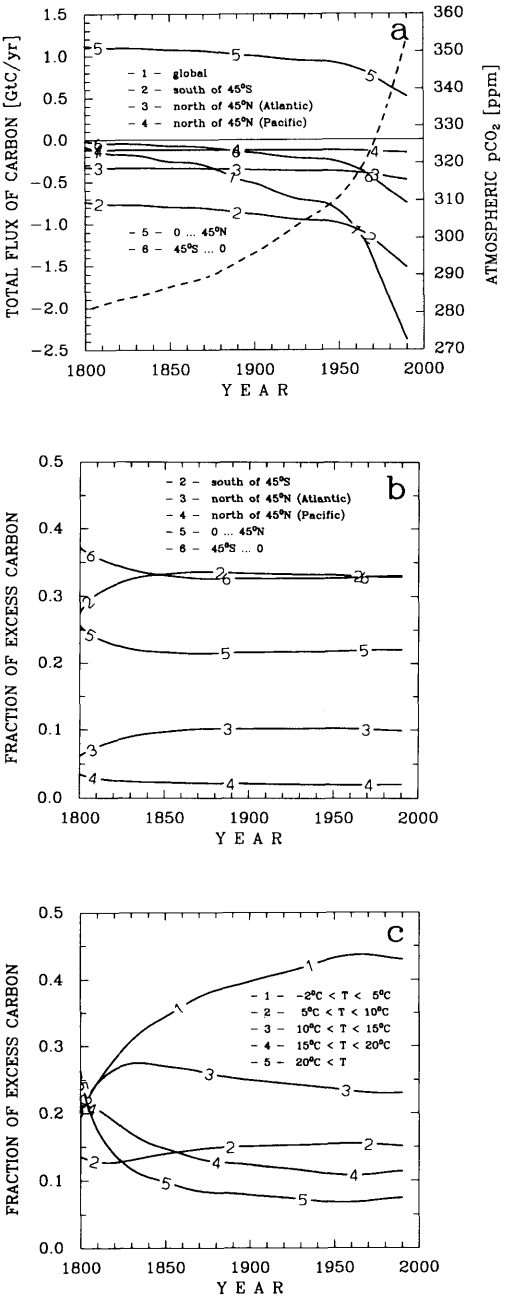

Fig. 5. Evolution of the total ocean-to-atmosphere carbon flux [GtC/yr], (a), during 1800–1990 AD in different latitude bands when the model is forced with the observed pCO_2^{atm} (dashed) and fractions of excess carbon uptake in different latitude bands, (b), and temperature ranges, (c). Circulation state A is used for the integration.

Ekman pumping in the low latitudes influences in a significant way the global uptake. If wind stress is switched off and upwelling at the equator is absent, total uptake is reduced by more than 20% in states D and E. Additional meridional mixing due to parameterization (1), on the other hand, has little effect on the uptake of total carbon.

The second most important region for uptake in this model is the Southern Ocean where, in all cases, over 30% of the excess carbon is sequestered by deep convection. The other region of deep water formation, the northern North Atlantic, is by far less important in taking up excess carbon and only accounts for about 10% of the total uptake. Uncertainties in the convection depth and rate of deep water formation thus have an appreciable effect on the estimates of global uptake. Changes in vertical transport processes (diffusion, advection, convection) in the region within 45° latitude of the equator and in the Southern Ocean should affect anthropogenic uptake rates the most. If vertical mixing in the former is reduced by switching off wind stress (states D and E), the thermocline becomes shallower (note the position of the 5°C isotherm in Fig. 6), vertical gradients in excess carbon are larger, and the uptake is reduced significantly (Table 5). Changing the north-south buoyancy contrast suppresses surface-to-bottom convection in the North Atlantic but has little influence on the global uptake (compare D, E and B, F) due to the relatively minor importance of this region for the global uptake. While uncertainties do exist, we note that the distribution of temperature and salinity in the deep Pacific and Atlantic in state A suggest that deep water formation in the North Atlantic and the Southern Ocean operates in about the right proportion, and the distribution of pre-industrial radiocarbon confirms that the absolute rates of water renewal (or overturning) in the three basins are reasonably represented in state A.

Excess carbon in the Atlantic demonstrates how sensitively the results depend on the processes described above (Fig. 6). The distributions can be compared with Maier-Reimer and Hasselmann (1987) and Sarmiento et al. (1992, their Fig. 8). Excess carbon of our "best" modern state (state A, Fig. 6a) compares fairly well with Maier-Reimer and Hasselmann (1987), except for the northern North Atlantic where the 1987-version of the Hamburg model is known to form too little

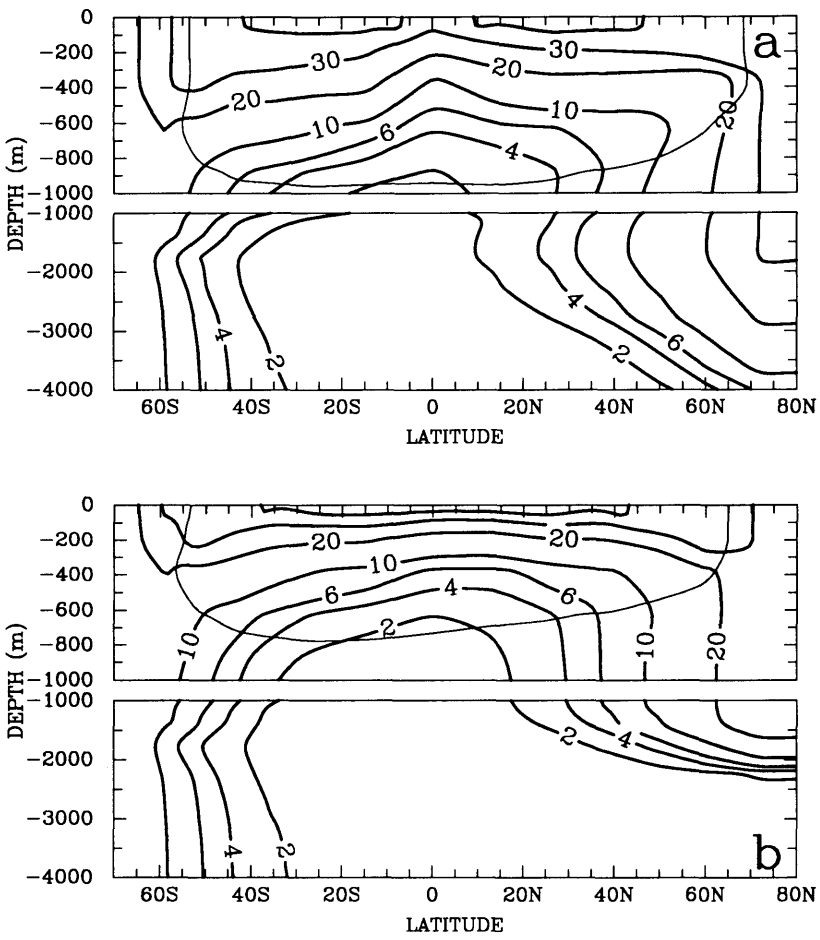

Fig. 6. Excess total carbon [μmole kg^{-1}] in the Atlantic Ocean in 1984 AD for the uptake experiment with state A, (a) and state E, (b). The 5°C isotherm is indicated by the thin line.

NADW. Because wind stirring is absent, excess carbon has penetrated far less deep within the top 1000 m for case E (Fig. 6b) than for case A. Convection, however, transports excess carbon in similar amounts into the deep ocean via the Southern Ocean. In the North Atlantic surface-to-bottom convection is suppressed in case A due to the altered north-south buoyancy contrast.

Contours of the perturbation fluxes as functions of time and latitude are given in Fig. 7 for states A and E. The three major uptake regions of both high latitudes and the low latitudes are apparent. Evidently, the relatively small surface area of the North Atlantic accounts for its reduced signal in the global uptake. Convection at high latitudes and upwelling at low latitudes (Ekman and thermohaline) are the vertical mixing processes that bring up "uncontaminated" waters which can take up excess carbon from the atmosphere. Meridional gradients are much reduced for state E (Fig. 7b) because of the absence of Ekman pumping in the low latitudes. As k is a constant, Fig. 7 also reflects the change in atmosphere-ocean partial pressure difference during this period. Minima of -39 ppm (65°S), -23 ppm (72°N) and -8.7 ppm at the equator in 1986 for state A compare well with Sarmiento et al. (1992, their Fig. 2a).

From the present results it is difficult to deter-

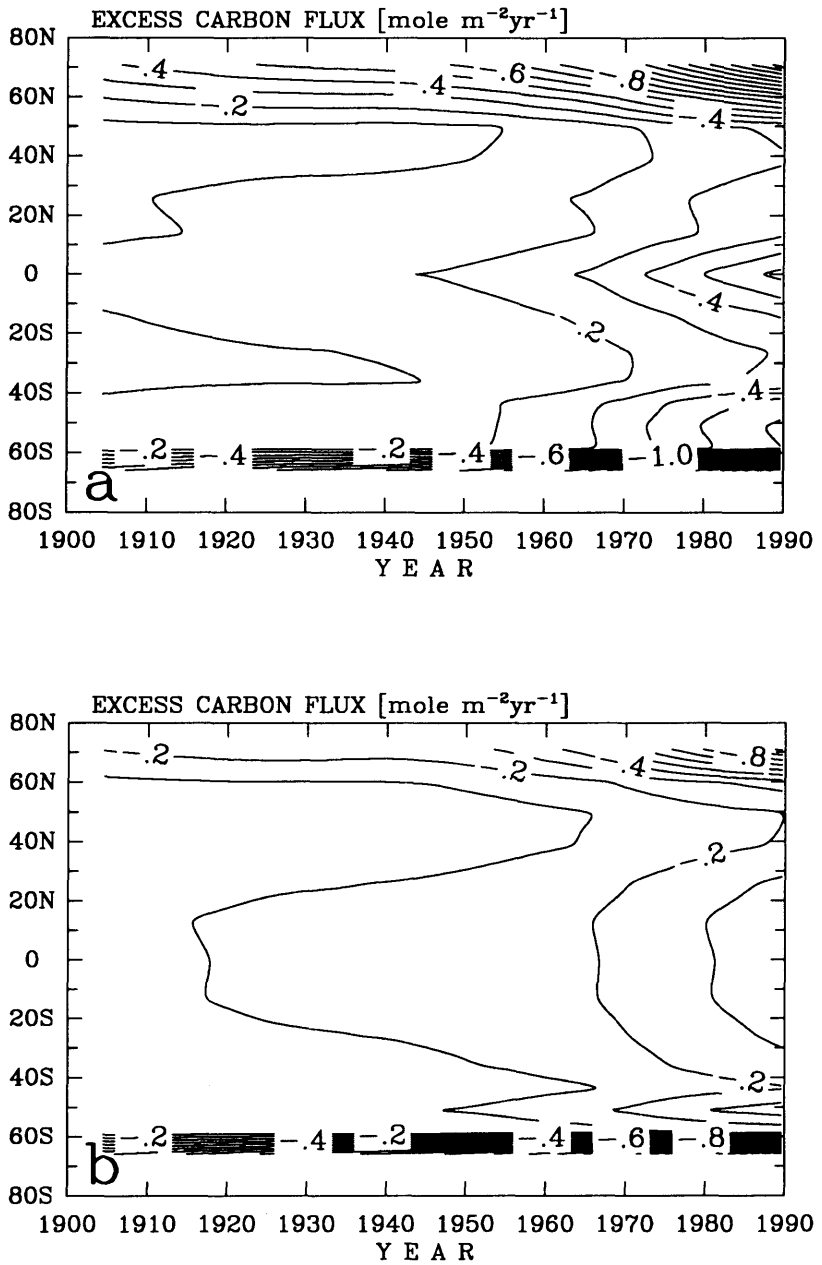

Fig. 7. Evolution of the global excess carbon flux as a function of latitude in mole m^{-2} yr^{-1}; negative fluxes are into the ocean. The regions of major uptake are related to high-latitude convection and Ekman pumping around the equator (a, state A). The latter mixing process is absent in state E, (b).

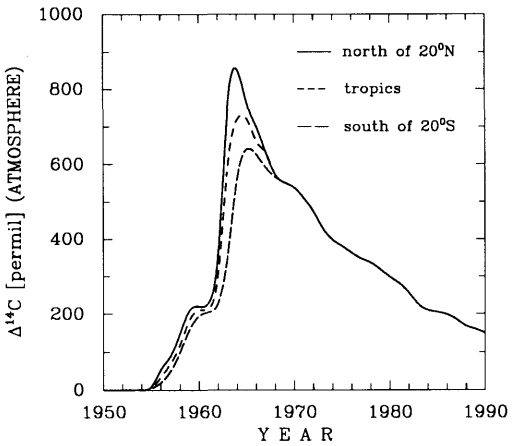

Fig. 8. Atmospheric $\Delta^{14}C$-values [$^{\circ}/_{oo}$] for 1950–1990 AD from Peng (pers. comm.) for latitudes south of 20° S (long dashed), the tropics (short dashed) and north of 20° N (solid).

mine whether state A, B or F exhibits a better overall performance with respect to tracer uptake. Additional constraints must therefore be used to check the quality of a particular steady state circulation. Below we will compare the uptake of bomb-produced radiocarbon and find a better performance for state A.

4. Bomb radiocarbon 1950–1990 AD

In Section 3, we have tested the capability of the model to simulate carbon uptake on time scales of a few centuries ($2\times CO_2$-experiments) to a few decades (industrial uptake) and found that results are sensitive to the parameterization of vertical and horizontal mixing processes. Uptake of bomb radiocarbon provides a further test of the model's performance on time scales of years to a few decades. Such experiments evidence possible problems related to tracer mixing vertically and horizontally in the top 500 m of the water column. It is emphasized that the present model is not suitable to study *variability* of the thermohaline circulation on time scales of decades and shorter because these are due to meridional advection of surface salinity anomalies by the wind-driven circulation (Winton and Sarachik, 1993). However, assuming a steady state circulation, it can nevertheless be used to estimate global uptake rates of tracers.

Radiocarbon in the ocean is usually reported as a normalised ratio of isotopic concentrations in $\Delta^{14}C$ units ($^{\circ}/_{oo}$), which are calculated according to

$$\Delta^{14}C = 1000\,\frac{^{14}C/^{12}C - {}^{14}C/^{12}C|_{std}}{^{14}C/^{12}C|_{std}}, \qquad (10)$$

where ^{14}C and ^{12}C are concentrations (in moles kg^{-1}) and a correction for isotopic fractionation ($\delta^{13}C = -25^{\circ}/_{oo}$) is assumed; $^{14}C/^{12}C|_{std} = 1.176\times10^{-12}$ is an international standard (Siegenthaler, 1989). Modelling radiocarbon in the ocean would therefore require carrying absolute concentrations of both ^{14}C and ^{12}C. However, Fiadeiro (1982) pointed out that the evolution of the $^{14}C/^{12}C$-ratio can be approximately described using eq. (2) directly for the ratio; nonlinear effects are small. Here, we treat this ratio like a concentration expressed in $\Delta^{14}C$ units ($^{\circ}/_{oo}$) following Maier-Reimer and Hasselmann (1987) and Toggweiler et al. (1989).

During spin-up the sea surface concentration is restored to $C^* = 1000^{\circ}/_{oo}$ on a time scale of 6 years to account for the long isotopic equilibration time of radiocarbon (Broecker and Peng, 1974). Toggweiler et al. (1989) have estimated a time scale of 5 years using the invasion rate of 20 mole C m^{-2} yr^{-1} with an average surface concentration of 2 mole C m^{-3} into a surface layer of 50 m depth. Here we use 6 years for the best tuned state A because the shorter equilibration time results in surface $\Delta^{14}C$ values that are too high and also increases total uptake significantly (see below).

For the bomb radiocarbon uptake experiment the evolution of the atmospheric $^{14}C/^{12}C$-ratio (Fig. 8) is taken from Broecker et al. (1985 and Peng, personal communication); before 1968 the ratio shows a latitudinal dependence which disappears later due to mixing in the atmosphere. In Table 6, the total bomb inventory and the distributions according to regions are given and compared to the GCM runs of Toggweiler et al. (1989) and the observational estimates of Broecker et al. (1985). Broad agreement of the uptake with circulation state A is found with the largest deviation in the Southern Ocean where, due to vigorous convection, the inventory is more than twice as large as the estimates of Broecker et al. (1985).

Table 6. *Bomb radiocarbon inventories in different ocean basins for the steady state circulations A–F of Fig. 2*

	A	B	C	D	E	F	P	obs.
Atlantic 1972	bomb inventory [10^9 atoms cm^{-2}]							
45°N–80°N	11.5	12.4	14.5	12.6	11.5	13.3	11.0	13.8
15°N–45°N	6.2	7.2	8.1	5.7	5.9	8.5	7.1	13.2
15°S–15°N	4.2	2.9	3.4	5.1	5.1	3.6	3.8	3.5
40°S–15°S	7.0	7.4	8.5	5.8	5.7	8.6	8.4	9.5
Pacific 1974	bomb inventory [10^9 atoms cm^{-2}]							
45°N–80°N	7.9	9.6	11.1	8.7	8.7	11.1	4.6	5.9
15°N–45°N	7.7	9.2	10.4	6.7	6.7	10.4	8.5	9.3
15°S–15°N	4.8	3.3	3.8	5.6	5.6	3.8	4.4	5.7
40°S–15°S	7.4	7.8	8.9	5.7	5.7	9.2	8.6	11.0
Indian 1978	bomb inventory [10^9 atoms cm^{-2}]							
40°S–20°N	6.4	6.2	6.9	5.8	5.8	7.0	8.6	8.5
S. Ocean 1974	bomb inventory [10^9 atoms cm^{-2}]							
70°S–40°S	8.2	8.9	10.4	9.2	9.2	10.5	4.6	4.4
Global	bomb inventory [10^{28} atoms]							
1975	2.6	2.7	3.1	2.6	2.5	3.1	2.4	2.9
1990	3.2	3.4	3.8	3.0	2.9	3.8	—	—

P represents the prognostic OGCM run of Toggweiler et al. (1989), and the observational estimates are from Broecker et al. (1985) as given in Toggweiler et al. (1989). The total uptake is also given for 1975 and 1990; note that the observational estimate is the sum over the different basins in different years. The model inventories have been calculated from $\Delta^{14}C$–$\Delta^{14}C$ (1950) multiplying it by $10^{-3} \times 1.176 \times 10^{-12} \times 2000$ μmoles kg$^{-1} \times$ 1027 kg m^{-3} assuming an average surface value of ΣC of 2000 μmoles kg^{-1}.

However, a recent observational study also indicates significantly higher bomb inventories in the Atlantic south of 60°S (Schlosser et al., 1994).

Uptake in the mid-latitudes of the North Atlantic is smaller than the observational estimate but very close to the GCM results. On the other hand, uptake in the North Pacific is too high due to convection (down to about 250 m) but because of the limited area, this is of minor importance. Note that the GCM results are in closer agreement with the observational estimates both in the Southern Ocean and the North Pacific. Total uptake in 1975 for state A is slightly larger than the value of the Princeton model but about 10% less than the observed. The restoring time scale and Ekman pumping most significantly influence global uptake of radiocarbon as can be seen by comparing states B, C and D.

The observed bomb inventory is a result of vertical mixing and gas exchange. The mean penetration depth, defined as the ratio of bomb inventory to surface $\Delta^{14}C$, is mainly influenced by the vertical transport and hence is a diagnostic tool to separate the two processes. The values are given in Table 7 and, again, reasonable qualitative agreement is found. Major differences occur in the Southern Ocean where convection seems too strong in this model and notably in the mid-latitudes where vertical transport is underestimated probably

Table 7. *Penetration depth for bomb radiocarbon in different ocean basins for the steady state circulations A–F of Fig. 2*

	A	B	C	D	E	F	obs.
Atlantic 1972	penetration depth [km]						
45°N–80°N	0.61	0.53	0.53	0.47	0.41	0.50	0.80
15°N–45°N	0.20	0.23	0.23	0.14	0.14	0.23	0.40
15°S–15°N	0.18	0.28	0.20	0.13	0.13	0.21	0.18
40°S–15°S	0.24	0.23	0.23	0.14	0.14	0.25	0.38
Pacific 1974	penetration depth [km]						
45°N–80°N	0.75	0.87	0.87	0.48	0.49	0.87	0.18
15°N–45°N	0.25	0.30	0.31	0.16	0.16	0.31	0.34
15°S–15°N	0.20	0.23	0.23	0.14	0.15	0.23	0.25
40°S–15°S	0.25	0.28	0.28	0.15	0.15	0.29	0.35
Indian 1978	penetration depth [km]						
40°S–20°N	0.23	0.24	0.24	0.17	0.17	0.25	0.32
S. Ocean 1974	penetration depth [km]						
70°S–40°S	0.57	0.61	0.61	0.34	0.33	0.71	0.33
Global	penetration depth [km]						
1975	0.29	0.32	0.32	0.19	0.19	0.33	—
1990	0.47	0.52	0.53	0.35	0.35	0.54	—

The observational estimates are from Broecker et al. (1985). The penetration depth is defined as the ratio of bomb inventory to surface concentration change. The observational estimate is calculated as the mean of the penetration depths reported in Broecker et al. (1985, Tabs. 1, 2 and 3).

due to ventilation caused by the wind-driven gyre circulation.

The surface $\Delta^{14}C$ values before the bomb and during the GEOSECS survey are displayed in Fig. 9 for Atlantic and Pacific using the best tuned circulation state A. The zonally averaged model captures the meridional structure and the transient nature of the surface concentration fairly well. Systematically larger values are seen at the pre-bomb steady state. It must be noted that the model starts with $\Delta^{14}C = 0‰$ thus ignoring the Suess effect. Inclusion of this effect would lower the model's $\Delta^{14}C$ surface values by about $25‰$ improving the agreement. The reason for higher bomb radiocarbon uptake for states C and F noted above lies in the fact that the surface concentrations are generally too large (Fig. 10) as a conse-

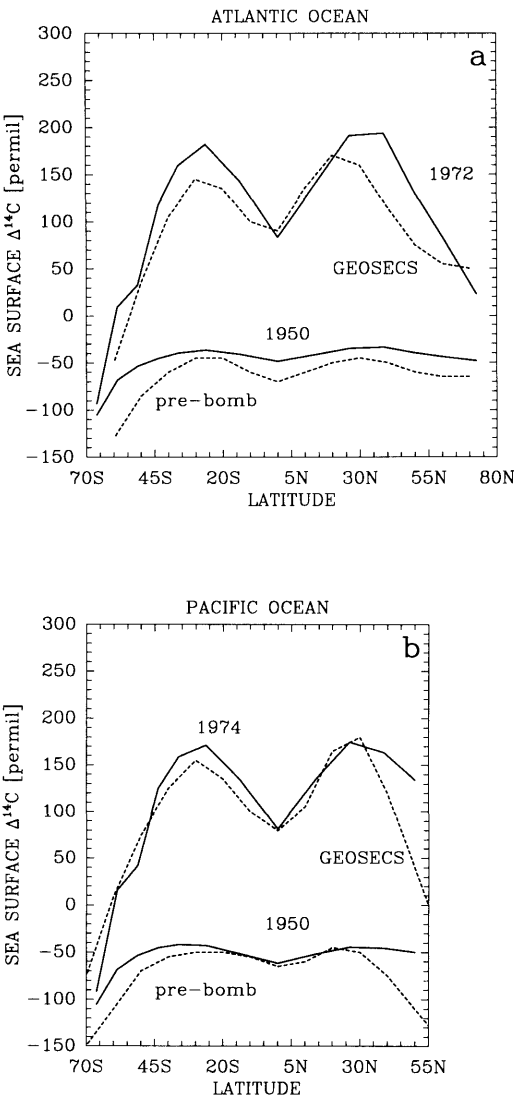

Fig. 9. Sea surface $\Delta^{14}C$-values for the Atlantic Ocean in 1950 and 1972, (a), the Pacific in 1950 and 1974, (b) for state A. The pre-bomb estimate and GEOSECS data of Broecker and Peng (1982) are given for comparison (dashed).

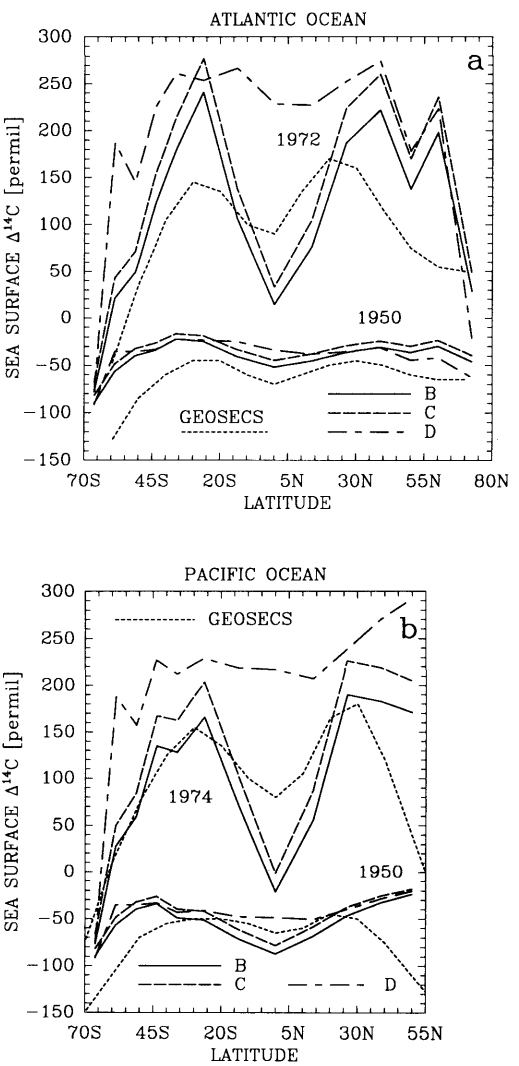

Fig. 10. As Fig. 9 for circulation states B, C, and D.

quence of the shorter restoring time for $\Delta^{14}C$ and wind-driven upwelling in low latitudes. In all states the model fails to reproduce the low values observed in the high southern latitudes of the Pacific. The same problem was observed in Stocker et al. (1992) and is related to the strong southward flow of "young" surface waters into the Southern Ocean. Also, $\Delta^{14}C$ is generally too high in the Pacific north of 30°N. It is interesting to note that the same discrepancy is observed in the 3-dimensional model of Toggweiler et al. (1989, their Fig. 6).

The surface values of $\Delta^{14}C$ for states B, C and D are given in Fig. 10 and emphasize the superiority of state A in simulating observed features. Increasing the restoring time for radiocarbon simply shifts the curve to lower values but does not influence its meridional structure (B, C). The exaggerated gradients of states B and C are highlighting the need for parameterization (1) accounting for meridional mixing due to the wind-driven gyre circulation. This deficiency is less important for sea surface temperature and salinity because they are restored to observations on a much shorter time scale (50 days). However, surface heat and freshwater fluxes are affected as shown in WS92.

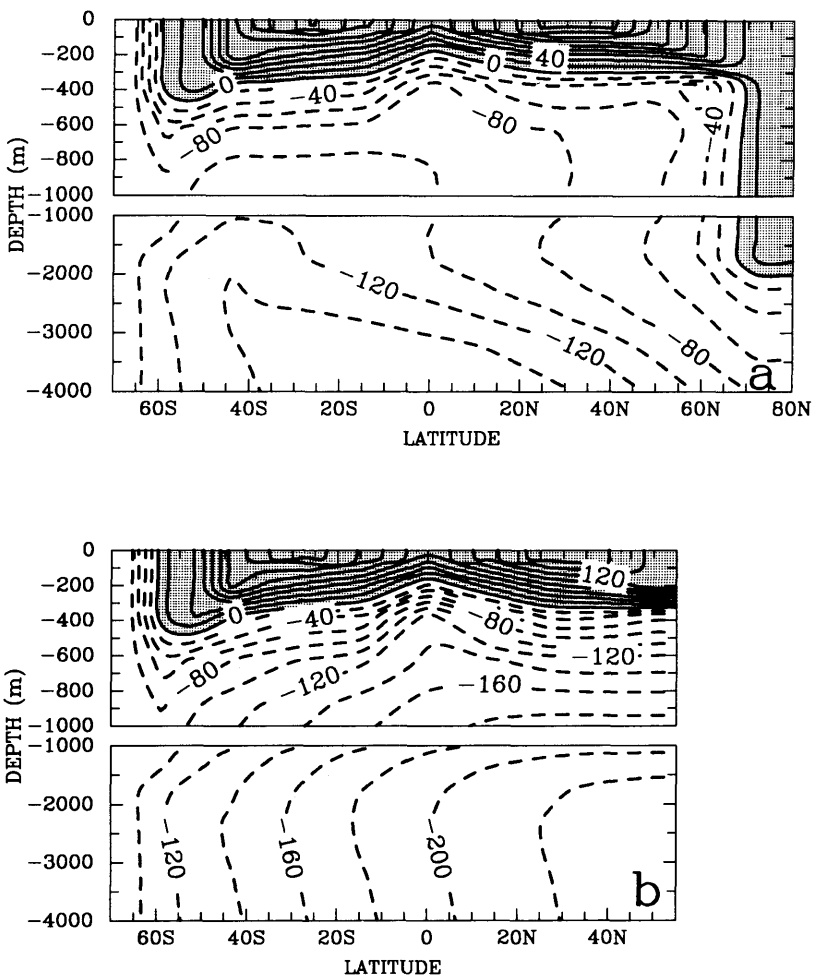

Fig. 11. Latitude-depth section of $\Delta^{14}C$ in the Atlantic (a, 1972) and the Pacific (b, 1974) for circulation state A.

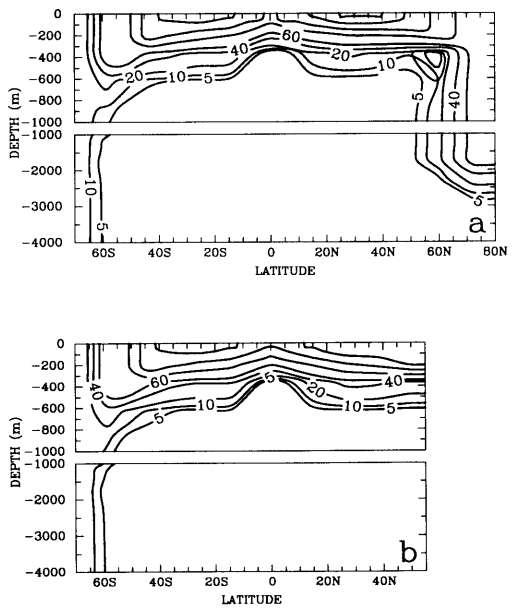

Fig. 12. Latitude-depth section of bomb-produced $\Delta^{14}C$ (i.e., Fig. 11 minus pre-bomb $\Delta^{14}C$) in the Atlantic (a, 1972) and the Pacific (b, 1974) for circulation state A.

The slow restoring time of radiocarbon and the relatively short integration interval (25 years of uptake) allow such gradients to develop in $\Delta^{14}C$. Inclusion of additional surface mixing removes this problem and does not influence the circulation much because the surface density is essentially fixed under restoring boundary conditions. Ekman pumping is also seen to be important in reducing $\Delta^{14}C$ to more realistic values in low latitudes (state D). While less evident in the pre-industrial steady state, the absence of Ekman induced upwelling of older waters is obvious in the bomb signal. This exercise demonstrates the usefulness of bomb calibration and shows that, if tracer uptake is to be simulated over short time scales (e.g., freons), the model must be calibrated beforehand. Only in this way can the absence of surface mixing processes that are important on time scales of decades and less be detected and accounted for by including additional parameterizations.

Latitude-depth sections of radiocarbon in the Atlantic (1972) and the Pacific (1974) are given in Fig. 11. The 0-contour can be compared to the sections from GEOSECS. The model gives an average depth about 400 m which agrees quite well with the observations. Deviations are present in the Southern Ocean where the model starts with too high steady state values and hence the 0-contour is located too deep. Strong convection in the North Atlantic is also transporting the bomb signal deeper into the ocean than observed although the inventory agrees quite well with the observational estimate (Table 6). For comparison with other perturbation models Fig. 12 shows the purely bomb-produced radiocarbon concentrations.

5. Conclusions

In this paper, we have presented an efficient physical-geochemical model in which tracer and carbon cycle components are coupled to a thermohaline circulation model of the world ocean. We have explored the model sensitivity of tracer transport in three different uptake experiments. Here, only an inorganic carbon cycle has been considered by carrying total carbon as a conservative tracer with alkalinity recovered from salinity. Using a well-tuned state consistent with the modern thermohaline circulation and a realistic gas exchange rate the evolution of the airborne fraction in a $2 \times CO_2$-experiment follows closely the results of 3-dimensional ocean general circulation models.

The importance of vertical mixing processes such as deep water formation in high latitudes and Ekman pumping in low latitudes for the uptake of excess carbon is quantitatively assessed. The total uptake is not very sensitive to the depth and strength of NADW formation within the range spanned by a weak and a strong conveyor belt, but the absence of surface wind stress results in a reduction of over 20% and changes the distribution of excess carbon significantly in the upper 1000 m. In an additional experiment where the convection depth in high southern latitudes was reduced from 4000 m to 2000 m, global uptake of carbon was about 10% smaller. For the most realistic circulation, state A, we found a global oceanic uptake from 1794–1990 AD of about 120 Gt C and an average atmosphere-to-ocean perturbation flux of 2.13 Gt C yr^{-1} from 1980–1989.

Meridional mixing in surface waters is not well represented in a model where the horizontal diffusivity is held constant with depth. The uptake of

bomb-produced radiocarbon showed that with an additional parameterization of surface mixing it was possible to achieve closer agreement with the observations. Although not apparent in temperature and salinity fields under restoring boundary conditions, the evolution of bomb radiocarbon reveals this deficiency because the equilibration time of radiocarbon is similar to the time scale of the gyral circulation which is an important component of near-surface meridional mixing. This 3-dimensional feature can be reasonably parameterized by introducing a depth-dependent horizontal diffusivity. The present model should be used for other tracer uptake experiments on decadal time scales only in conjunction with such a calibration.

Over 30 % of excess carbon uptake in this model occurs in the Southern Ocean. Bomb uptake experiments, however, have shown that the penetration depth is about twice the observational estimate in this region. This suggests that the surface-to-deep exchange in the Southern Ocean is a potentially weak point of the present model and that the global uptake rates are likely upper estimates. Also 3-dimensional models show disagreement mainly in this region. While the Hamburg model sequesters excess carbon in the Southern Ocean by convection similar to our model, the Princeton model has much weaker convection there and hence a smaller global uptake.

The next step is to incorporate an organic carbon cycle model that includes a representation of the vertical particulate carbon flux. Additionally, the ocean-to-atmosphere fluxes of the different carbon isotopes must be modelled including fractionation effects and using formulation (7) in conjunction with standard isotope ratios. The organic carbon cycle, in its simplest form, requires three additional tracers, alkalinity, phosphate and oxygen and a formulation of chemical interactions between these species (Bacastow and Meier-Reimer, 1990). This implementation is in progress and necessary before the problem of pCO_2 variations during rapid changes of the ocean's thermohaline circulation can be addressed with this model.

6. Acknowledgements

We have benefited from discussions with David Archer. Thanks are due to Martin Heimann, Fortunat Joos and Tsung-Hung Peng who provided the Siple/Mauna Loa pCO_2-data and the atmospheric $\Delta^{14}C$ concentrations. The comments of Ernst Maier-Reimer and Uli Siegenthaler and an anonymous reviewer have helped improve this paper. This study was made possible by grant DE-FG02-91ER61202 of the U.S. Department of Energy. This is Lamont-Doherty Earth Observatory contribution 5137.

REFERENCES

Bacastow, R. and Maier-Reimer, E. 1990. Ocean-circulation model of the carbon cycle. *Climate Dyn.* **4**, 95–125.

Bolin, B., Björkström, A. and Holmen, K. 1983. The simultaneous use of tracers for ocean circulation studies. *Tellus* **35B**, 206–236.

Broecker, W. S. and Denton, G. H. 1989. The role of ocean-atmosphere reorganizations in glacial cycles. *Geochim. Cosmochim. Acta* **53**, 2465–2501.

Broecker, W. S. and Peng, T.-H. 1974. Gas exchange rates between air and sea. *Tellus* **26**, 21–35.

Broecker, W. S. and Peng, T.-H. 1982. *Tracers in the sea.* Eldigio Press, Lamont-Doherty Earth Observatory, Palisades, NY.

Broecker, W. S. and Peng, T.-H. 1992. Interhemispheric transport of carbon dioxide by ocean circulation. *Nature* **356**, 587–589.

Broecker, W. S., Peng, T.-H., Östlund, G. and Stuiver, M. 1985. The distribution of bomb radiocarbon in the ocean. *J. Geophys. Res.* **90**, 6953–6970.

Bryan, F. 1986. High-latitude salinity effects and interhemispheric thermohaline circulations. *Nature* **323**, 301–304.

Culkin, F. 1965. The major constituents of sea water. In: *Chemical oceanography* (eds. J. P. Riley and G. Skirrow), vol. 1. Academic, 121–161.

Fiadeiro, M. E. 1982. Three-dimensional modeling of tracers in the deep Pacific Ocean (II). Radiocarbon and the circulation. *J. Marine Res.* **40**, 537–550.

Heinze, C., Maier-Reimer, E. and Winn, K. 1991. Glacial pCO_2 reduction by the world ocean: experiments with the Hamburg carbon cycle model. *Paleoceanography* **6**, 395–430.

Levitus, S. 1982. *Climatological atlas of the world ocean.* NOAA Prof. Paper 13, US Govt. Printing Office, Washington DC, 173 pp.

Maier-Reimer, E. and Hasselmann, K. 1987. Transport and storage of CO_2 in the ocean, an inorganic ocean-circulation carbon cycle model. *Climate Dyn.* **2**, 63–90.

Maier-Reimer E. and Mikolajewicz, U. 1989. *Experiments with an OCGM on the cause of the Younger Dryas.* Max Planck Institut für Meteorologie, Hamburg, Germany, 39, 13 p.

Manabe, S. and Stouffer, R. J. 1993. Century-scale effects of increased atmospheric CO_2 on the ocean-atmosphere system. *Nature* **364**, 215–218.

Marotzke, J., Welander, P. and Willebrand, J. 1988. Instability and multiple equilibria in a meridional-plane model of the thermohaline circulation. *Tellus* **40A**, 162–172.

Mehrbach, C., Culberson, C. H., Hawley, J. E. and Pytkowicz, R. M. 1973. Measurement of the apparent dissociation constants of carbonic acid in seawater at atmospheric pressure. *Limnology and Oceanogr.* **18**, 897–907.

Menard, H. W. and Smith, S. M. 1966. Hypsometry of ocean basin provinces. *J. Geophys. Res.* **71**, 4305–4325.

Mysak L. A., Stocker, T. F. and Huang, F. 1993. Century-scale variability in a randomly forced, two-dimensional thermohaline ocean circulation model. *Climate Dyn.* **8**, 103-116.

Oeschger, H., Siegenthaler, U., Schotterer, U. and Gugelmann, A. 1975. A box diffusion model to study the carbon dioxide exchange in nature. *Tellus* **27**, 168–192.

Sarmiento, J. L., Orr, J. C. and Siegenthaler, U. 1992. A perturbation simulation of CO_2 uptake in an ocean general circulation model. *J. Geophys. Res.* **97**, 3621–3645.

Schlosser, P., Kromer, B., Weppernig, R., Loosli, H. H., Bayer, R., Bonani, G. and Suter, M. 1994. The distribution of ^{14}C and ^{39}Ar in the Weddell Sea. *J. Geophys. Res.*, in press.

Siegenthaler, U. 1983. Uptake and excess CO_2 by an outcrop-diffusion model of the ocean. *J. Geophys. Res.* **88**, 3599–3608.

Siegenthaler, U. 1989. Carbon-14 in the oceans. In: *Handbook of environmental isotope geochemistry* (eds. P. Fritz and J. Ch. Fontes), vol. 3. Elsevier, 75–137.

Siegenthaler, U. and Oeschger, H. 1987. Biospheric CO_2 emissions during the past 200 years reconstructed by deconvolution of ice core data. *Tellus* **39B**, 140–154.

Siegenthaler, U. and Joos, F. 1992. Use of a simple model for studying oceanic tracer distributions and the global carbon cycle. *Tellus* **44B**, 186–207.

Stocker, T. F., Wright, D. G. and Mysak, L. A. 1992a. A zonally averaged, coupled ocean-atmosphere model for paleoclimatic studies. *J. Climate* **5**, 773–797.

Stocker, T. F., Wright, D. G. and Broecker, W. S. 1992b. The influence of high-latitude surface forcing on the global thermohaline circulation. *Paleoceanography* **7**, 529–541.

Sundquist, E. T. 1985. Geological perspectives on carbon dioxide and the carbon cycle. In: *The carbon cycle and atmospheric CO_2: Natural variations archean to present* (eds. E. T. Sundquist and W. S. Broecker). Geophys. Monogr., vol. 32, Am. Geophys. Union, 5–59.

Takahashi, T., Broecker, W. S., Bainbridge, A. E. and Weiss, R. F. 1980. *Carbonate chemistry of the Atlantic, Pacific and Indian Oceans. The results of the GEOSECS expeditions, 1972–1978.* Lamont-Doherty Geological Observatory, Tech. Rep., CV-1-80, 196 p.

Takahashi, T., Broecker, W. S. and Bainbridge, A. E. 1981. The alkalinity and total carbon dioxide concentration in the world ocean. In: *Carbon cycle modelling, Scope 16*, (ed. B. Bolin). Wiley, 271–286.

Tans, P. P., Fung, I. Y. and Takahashi, T. 1990. Observational constraints on the global atmospheric CO_2 budget. *Science* **247**, 1431–1438.

Toggweiler, J. R., Dixon, K. and Bryan, K. 1989. Simulations of radiocarbon in a coarse-resolution world ocean model, 2. Distributions of bomb-produced carbon 14. *J. Geophys. Res.* **94**, 8243–8264, 1989.

Weiss, R. F. 1974. Carbon dioxide in water and seawater: the solubility of a non-ideal gas. *Mar. Chem.* **2**, 203–215.

Winton, M. and Sarachik, E. S. 1993. Thermohaline oscillations induced by strong steady salinity forcing of ocean general circulation models. *J. Phys. Oceanogr.* **23**, 1389–1410.

Wright, D. G. and Stocker, T. F. 1991. A zonally averaged ocean model for the thermohaline circulation. Part I: Model development and flow dynamics. *J. Phys. Oceanogr.* **21**, 1713–1724.

Wright, D. G. and Stocker, T. F. 1992. Sensitivities of a zonally averaged global ocean circulation model. *J. Geophys. Res.* **97**, 12707–12730.